Proceedings of the Eighth (1998) International Offshore and Polar Engineering Conference
Montréal, Canada, May 24-29, 1998

ISBN 1-880653-34-6 (Set); ISBN 1-880653-37-0 (Vol. III)

Numerical Study of Solitary Wave on a Mild Slope

Chung-Ren Chou
National Taiwan Ocean University
Keelung, Taiwan, China

Ouyang Kwan
China Junior College of Marine Technology
Taipei, Taiwan, China

Abstract

To assess the generation, propagation, deformation and breaking of the solitary wave on a mild slope, a numerical simulation of the wave making problem by a boundary element method is developed in this paper. The numerical scheme involved is based on Lagrangian description together with a finite difference approximation of the time derivatives. The simulation of this study concerns of solitary wave propagating from constant depth and over a mild slope. The time history of the solitary wave propagation is shown and the numerical results of mass, potential energy and kinetic energy of the fluid are presented to confirm its accuracy.

Key word: boundary element, numerical tank, solitary wave, breaking wave, Lagrangian description, time history

1. Introduction

When water waves reach coastal regions, it is observed that an increase in wave height and a decrease in wavelength occurs due to the reduction of water depth. This phenomenon makes wave steeper towards the shore and leads to wave instability and breaking. For the sediment transport by coastal current, shaping of beaches, and design of coastal structures used for beach protection, knowledge of the crest height or location of breaking wave is important in coastal engineering.

Numerical studies of solitary wave in shallow water have been developed by many researchers. The first discussion in detail for the propagation of solitary wave on a slope was made by Madsen and Mei (1969). Based on a set of approximate equations for long wave, the numerical results in that study were compared with experimental date and a reasonable agreement was obtained. To describe the development of solitary wave moving onto a shelf, numerical solutions of a variable-coefficient Korteweg-de Vries equation was derived by Johnson (1972). Nakayama (1983) discussed the transformation of solitary wave and the running up against a vertical wall by means of a boundary element method. Using the nonlinear initial boundary condition and the velocity potential, the numerical wave generator was studied by Grilli and Subramanya (1989). By the boundary element method with the mixed Eulerian-Lagrangian description, Sugino and Tosaka (1990) analyzed the generation, propagation and deformation of a solitary wave in water tank with a gentle slope. Chou and Shih(1996) studied the propagation and deformation of solitary wave with submerged obstacles by using the boundary element method together with time derivative.

In this paper, the numerical results for the generation, propagation, and breaking of solitary wave on a mild slope are studied by boundary element method. The numerical scheme in this paper is based on the Lagrangian description together with the time derivative. To simulate the generation of solitary wave, the pseudo wave generator of piston type is chosen.

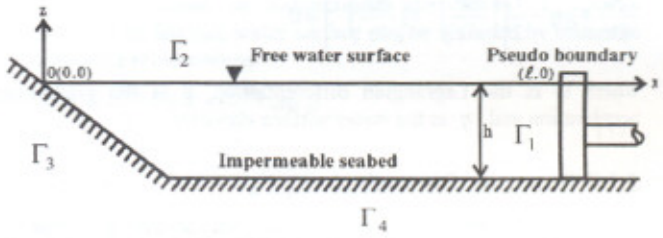

Fig. 1 Sketch of the water tank

2. Theoretical analysis

As shown in Fig. 1, the original coordinate system is located on the still water surface with x-axis pointed positively to pseudo wave generator and z-axis pointed positively upwards. The flow field is bounded by a numerical wave generator boundary Γ_1, a free water surface Γ_2, a slope Γ_3 and horizontal impermeable seabed Γ_4. For an inviscid and incompressible flow, the flow motion has a velocity potential $\Phi(x,z;t)$ satisfying the Laplace equation if it is irrotational. The expression can be written as

$$\partial x^2 + \partial z^2 = 0 \tag{1}$$

2.1 Boundary conditions

2.1.1 Wave generator boundary Γ_1 :

In this paper, the wave generator is assumed to be a piston type. For continuity, the horizontal velocity of wave-making paddle, $U(t)$, and the fluid velocity have the following relationship:

$$\overline{\Phi} = \frac{\partial \Phi}{\partial n} = -U(t) \tag{2}$$

where n denotes the normal unit vector. For simulating solitary wave, the U(t) can be expressed as

$$\begin{aligned} U(t) &= x_0 .\omega .\sec h^2[\omega(t-t_c)] \\ x_0 &= h\sqrt{\frac{4\varsigma_0}{3(h+\varsigma_0)}} \\ \omega &= \sqrt{\frac{g}{h}}\sqrt{\frac{3\varsigma_0}{4h}\left(1+\frac{\varsigma_0}{h}\right)} \\ t_c &= \frac{\pi}{\omega} \end{aligned} \tag{3}$$

where x_0 is the semistroke of the wave-making paddle and ς_0 is the wave height of solitary wave simulated.

2.1.2 Free water surface Γ_2

Assuming that the atmospheric pressure on free water surface is equal to zero, the following relationships can be obtained from the kinematic and dynamic conditions.

$$u = \frac{Dx}{Dt} = \frac{\partial \Phi}{\partial x} \tag{4}$$

$$w = \frac{Dz}{Dt} = \frac{\partial \Phi}{\partial z} \tag{5}$$

$$\frac{D\Phi}{Dt} + g\eta - \frac{1}{2}\left[\left(\frac{\partial \Phi}{\partial x}\right)^2 + \left(\frac{\partial \Phi}{\partial z}\right)^2\right] = 0 \tag{6}$$

where D is the Lagrangian differentiation, g is the gravitational acceleration and η is the water surface elevation.

2.1.3 Impermeable seabed Γ_3, Γ_4

Since the boundaries of seabed are assumed to be impermeable, the fluid velocity normal to the boundary has to be null, thus we have

$$\frac{\partial \Phi}{\partial n} = 0 \tag{7}$$

2.2 Integral Equation

According to Green's Second Identity, the velocity potential, $\Phi(x,z;t)$, at any point within the domain of computation can be obtained by the velocity potential on the boundary, $\Phi(\xi,\eta;t)$, and its normal derivative, $\partial\Phi(\xi,\eta;t)/\partial n$, that is

$$\Phi(x,z,t) = \frac{1}{2\pi}\int_\Gamma \left[\frac{\partial}{\partial n}\ln r - \Phi(\xi,\eta,t)\frac{\partial}{\partial n}\ln r \right] ds \tag{8}$$

where Γ denotes the boundary of computational region and $r = \left[(\xi - x)^2 - (\eta - z)^2\right]^{1/2}$.

When the inner point (x,z) is very close to the boundary point, (ξ', η'), the velocity potential of that point, $\Phi(\xi', \eta'; t)$, can be expressed as

$$\Phi(\xi',\eta';t) = \frac{1}{\pi}\int_\Gamma \left[\frac{\partial \Phi(\xi,\eta,t)}{\partial n}\ln\frac{1}{R} - \Phi(\xi,\eta;t)\frac{\partial}{\partial n}\ln\frac{1}{R} \right] ds \tag{9}$$

where $R = \left[\left(\xi - \xi'\right)^2 + \left(\eta - \eta'\right)^2\right]^{1/2}$.

To discretize the integral equation, the boundaries are divided into several linear elements with the introduction of local dimensionless coordinate, and Eq. (9) can be expressed as

$$\begin{aligned} \Phi_i(\xi',\eta';t) + \frac{1}{\pi}\sum_{j=1}^{N}\int_{\Gamma_j}\left[\Phi_j(\xi,\eta,t)M_1 + \Phi_{j+1}(\xi,\eta,t)M_2\right]\frac{\partial}{\partial n}\ln\frac{1}{R}ds \\ = \frac{1}{\pi}\sum_{j=1}^{N}\int_{\Gamma_j}\left[\overline{\Phi}_j(\xi,\eta,t)M_1 + \overline{\Phi}_{j+1}(\xi,\eta,t)M_2\right]\ln\frac{1}{R}ds \end{aligned} \tag{10}$$

$$M_1 = \frac{1-\chi}{2}, \quad M_2 = \frac{1+\chi}{2} \tag{11}$$

where M_1, M_2 denote shape functions, χ is the local dimensionless coordinate. Let

$$\begin{aligned} \frac{1}{\pi}\int_{\Gamma_j}\left[\Phi_j(\xi,\eta,t)M_1 + \Phi_{j+1}(\xi,\eta,t)M_2\right]\frac{\partial}{\partial n}\ln\frac{1}{R}ds &= \begin{bmatrix} h_{ij}^1 & h_{ij}^2 \end{bmatrix}\begin{bmatrix} \Phi_j \\ \Phi_{j+1} \end{bmatrix} \\ \frac{1}{\pi}\int_{\Gamma_j}\left[\overline{\Phi}_j(\xi,\eta,t)M_1 + \overline{\Phi}_{j+1}(\xi,\eta,t)M_2\right]\ln\frac{1}{R}ds &= \begin{bmatrix} g_{ij}^1 & g_{ij}^2 \end{bmatrix}\begin{bmatrix} \overline{\Phi}_j \\ \overline{\Phi}_{j+1} \end{bmatrix} \end{aligned} \tag{12}$$

and substitute Eq. (12) into Eq. (10), Eq. (10) can be expressed as a matrix foorm:

$$[\Phi] = [O][\overline{\Phi}] \tag{13}$$

$$[\Phi] = \Phi_i, \quad (i = 1 \sim N) \tag{14}$$

$$[\overline{\Phi}] = \overline{\Phi}_i = \frac{\partial \Phi_i}{\partial n}, \quad (i = 1 \sim N) \tag{15}$$

$$[O] = [H + I]^{-1}[G] \tag{16}$$

$$[H] = H_{ij}, \quad (i, j = 1 \sim N) \tag{17}$$

$$[G] = G_{ij}, \quad (i, j = 1 \sim N) \tag{18}$$

$$H_{ij} = \begin{cases} \overline{H}_{ij} & (i \neq j) \\ \overline{H}_{ij} + 1 & (i = j) \end{cases} \tag{19}$$

$$\overline{H}_{ij} = \begin{cases} h_{ij}^1 + h_{ij-1}^2 & (j \geq 2) \\ h_{i1}^1 + h_{iN}^2 & (j = 1) \end{cases} \tag{20}$$

$$G_{ij} = \begin{cases} g_{ij}^1 + g_{ij-1}^2 & (j \geq 2) \\ g_{i1}^1 + g_{iN}^2 & (j = 1) \end{cases} \tag{21}$$

where $[\Phi]$ is the potential function, $[\Phi]$ is the normal derivative of potential function on the boundary, $[O]$ is a matrix of the related shape function.

For substituting the boundaries conditions into Eq.(13) conveniently, we rewrite the matrix in Eq. (13) again as follow:

$$[\Phi_i] = [O_{ij}][\overline{\Phi}_i] \qquad i,j = 1 \sim 4 \tag{22}$$

where i,j denote different boundaries, $\Gamma_1, \Gamma_2, \Gamma_3$ and Γ_4. The numerical scheme has been discussed in detail by Chou(1983), Chou and Shih(1996).

2.3 Compatible equations

2.3.1 Initial conditions on boundaries

At the beginning of wave generation, i.e. t=0, the boundary conditions are expressed as follows:

(1) Numerical wave generator boundary Γ_1:

Based on the fact that the fluid velocity is the same as the horizontal velocity of the wave paddle, we can express the relationship as

$$\overline{\Phi}_1^k = \frac{\partial \Phi_1^k}{\partial n} = -\mathrm{U}(k) \tag{23}$$

For k=0,

$$\overline{\Phi}_1^0 = \frac{\partial \Phi_1^0}{\partial n} = -\mathrm{U}(0) \tag{24}$$

where the subscript "0" denotes the time of t=0.

(2) Free water surface Γ_2:

Assuming that the free water surface is still at t=0, the velocity potential on boundary is therefore

$$\Phi_2^0 = 0 \tag{25}$$

(3) Impermeable seabed Γ_3 and Γ_4:

Because the seabed is assumed impermeable, the velocity normal to the boundary is always null at any time:

$$\overline{\Phi}_i^k = \frac{\partial \Phi_i^k}{\partial n} = 0 \qquad i = 3,4 \qquad k = 0,1,2,\ldots \tag{26}$$

where k denotes level of time.

2.3.2 The finite difference approximation

At any time (t=kΔt), based on the weighted central difference, the tangential derivative of velocity potential on the free water surface can be obtained:

$$\left(\frac{\partial \Phi_{2,j}^k}{\partial s}\right) = \left(\frac{\Delta s_{j-1}^k}{\Delta s_j^k}\right)\frac{\Phi_{2,j+1}^k}{s'} + \left(\Delta s_j^k - \Delta s_{j-1}^k\right)\frac{\Phi_{2,j}^k}{s''} - \left(\frac{\Delta s_j^k}{\Delta s_{j-1}^k}\right)\frac{\Phi_{2,j-1}^k}{s'} \tag{27}$$

where

$$\Delta s_j^k = \sqrt{\left(x_{j+1}^k - x_j^k\right)^2 + \left(z_{j+1}^k - z_j^k\right)^2}$$

$$s' = \Delta s_j^k + \Delta s_{j-1}^k, \qquad s'' = \Delta s_j^k \cdot \Delta s_{j-1}^k$$

Differentiating the time derivative in Eq. (4) and Eq. (5) by orward-difference, we can obtain the new positions of elements on free water surface at next time

$$x^{k+1} = x^k + \left(\frac{\partial \Phi_2^k}{\partial x}\right)\Delta t$$

$$z^{k+1} = z^k + \left(\frac{\partial \Phi_2^k}{\partial z}\right)\Delta t \tag{28}$$

and get the new velocity potential on free water surface at next time from Eq.(6):

$$\Phi_2^{k+1} = \Phi_2^k + \frac{1}{2}\left[\left(\frac{\partial \Phi_2}{\partial s}\right)^2 + \left(\frac{\partial \Phi_2}{\partial n}\right)^2\right]^k \Delta t - g z^{k+1}\Delta t \tag{29}$$

Substituting Eq. (2), Eq. (7), and above equation into Eq. (22), we can obtain the following simultaneous equations:

$$\begin{bmatrix} \Phi_1 \\ \overline{\Phi}_2 \\ \Phi_3 \\ \Phi_4 \end{bmatrix}^{k+1} = \begin{bmatrix} I & -O_{12} & 0 & 0 \\ 0 & -O_{22} & 0 & 0 \\ 0 & -O_{32} & I & 0 \\ 0 & -O_{42} & 0 & I \end{bmatrix}^{-1} \begin{bmatrix} O_{11} & 0 & O_{13} & O_{14} \\ O_{21} & -I & O_{23} & O_{24} \\ O_{31} & 0 & O_{33} & O_{34} \\ O_{41} & 0 & O_{43} & O_{44} \end{bmatrix} \begin{bmatrix} \overline{\Phi}_1 \\ \Phi_2 \\ \overline{\Phi}_3 \\ \overline{\Phi}_4 \end{bmatrix}^{k+1} \tag{30}$$

2.3.3 Computational procedure

The iterative computational procedure is stated below:

(1) At $t = k\Delta t$, Eq. (24) to Eq. (26) are used to obtain the normal derivative of velocity potential on numerical wave generator boundary, $\overline{\Phi}_1^k$, on impermeable seabed, $\overline{\Phi}_3^k, \overline{\Phi}_4^k$, and the velocity potential on free water surface, Φ_2^k respectively. Substituting those values into Eq. (22), we can obtain the velocity potential on numerical wave generator boundary, Φ_1^k, on impermeable seabed, Φ_3^k, Φ_4^k, and the normal derivation of velocity potential on free water surface, $\overline{\Phi}_2^k$.

(2) From Eq.(27), we can get the tangential derivative of velocity potential on free water surface, $\partial \Phi_2^k / \partial s$.

(3) The x-directional or z-directional derivatives of velocity potential on the free water surface can be obtained by using the following relationships.

$$\frac{\partial \Phi_2}{\partial x} = \frac{\partial \Phi_2}{\partial n}\sin\beta - \frac{\partial \Phi_2}{\partial s}\cos\beta$$

$$\frac{\partial \Phi_2}{\partial z} = \frac{\partial \Phi_2}{\partial n}\cos\beta + \frac{\partial \Phi_2}{\partial s}\sin\beta \tag{31}$$

where β denotes the angle between the tangential direction of free water surface and the x-axis.

(4) From Eq. (28) or Eq. (29), the new position, x^{k+1}, z^{k+1}, or velocity potential on free water surface, Φ_2^{k+1}, at $t = (k+1)\Delta t$ can be obtained respectively.

(5) Using the new profile of the free water surface and new position of numerical wave-paddle, new $[O_{ij}]$ in Eq. (22) can be obtained by recalculating it.

(6) Substituting $\overline{\Phi}_1^{k+1}, \Phi_2^{k+1}, \overline{\Phi}_3^{k+1}, \overline{\Phi}_4^{k+1}$ into Eq. (30), we can obtain the new normal derivative of velocity potential on free water surface, $\overline{\Phi}_2^{k+1}$, the velocity potential on numerical wave

generator and impermeable boundaries, $\Phi_1^{k+1}, \Phi_3^{k+1}, \Phi_4^{k+1}$.

(7) By repeating procedure 2 through 6, the time history for the generation, propagation and deformation of wave can be simulated.

3.Numerical results

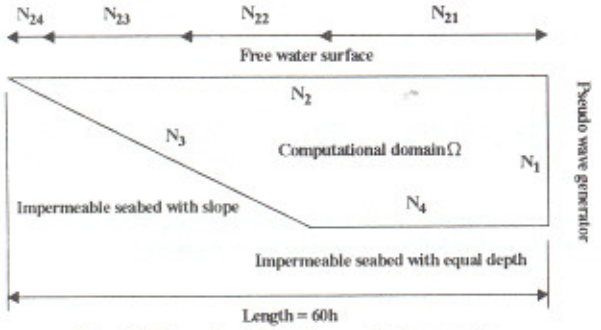

Fig. 2 The distribution of elements

The distribution of elements on the boundaries is shown in Fig. 2. To simulate more effectively the deformation and breaking of the solitary wave, an arbitrary discretization on the free water surface is applied.

In this study, the incident relative wave height is $\varsigma_0/h = 0.3$, while the length and slope of numerical tank are 60m and 1:30 respectively.

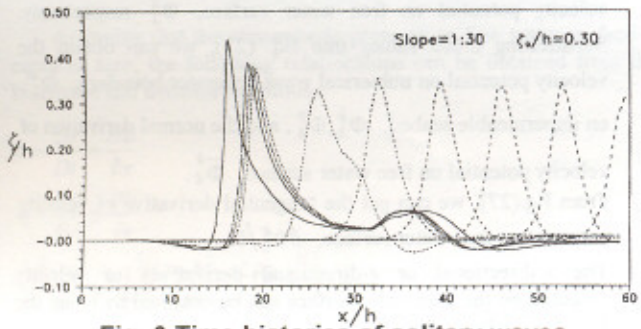

Fig. 3 Time histories of solitary waves

The time history of solitary wave is shown in Fig. 3. These profiles of wave are simulated at times: $t = 200\Delta t$, $t = 400\Delta t$, $t = 600\Delta t$, $t = 800\Delta t$, $t = 1000\Delta t$, $t = 1800\Delta t$, $t = 2600\Delta t$, $t = 2650\Delta t$, $t = 2700\Delta t$, $t = 3020\Delta t$ .The height and depth of breaking wave are about $\varsigma_b = 0.42, h_b = 0.53$, and $\varsigma_b/h_b = 0.79$. It is observed that an increase in wave height and a decrease in wave length occurs due to the reduction in water depth. The wave become steeper toward the shore and lead to instability and breaking.

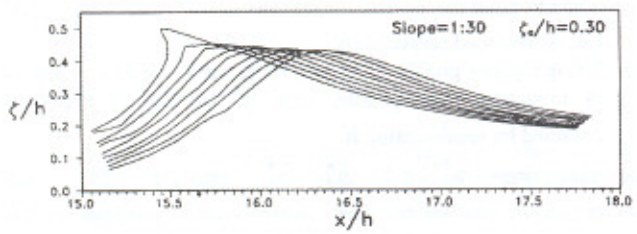

Fig. 4 The breaking of solitary wave

As shown in Fig. 4, the profiles of breaking wave are studied at times: $t = 2970\Delta t$, $t = 2980\Delta t$, $t = 2990\Delta t$, $t = 3000\Delta t$, $t = 3010\Delta t$, $t = 3020\Delta t$. In this figure, it is observed that the velocities of water particle on crest of the wave are faster than the velocity of solitary wave and lead to breaking.

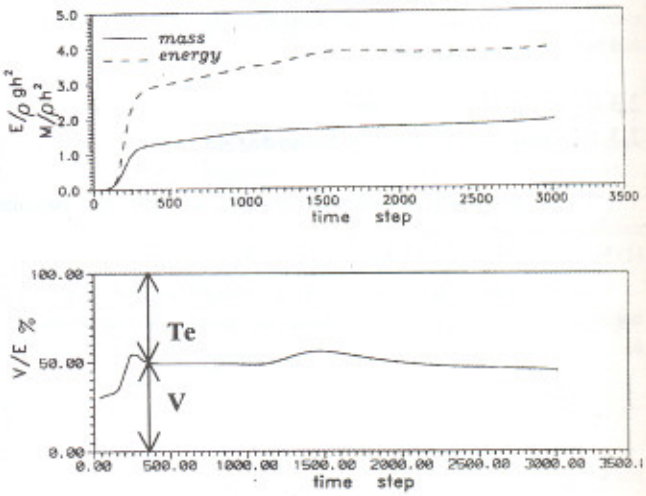

Fig.5 Variation of mass and energy

As shown in Fig.5, the mass, potential energy, and kinetic energy of fluid are studied to confirm the accuracy of numerical results. It is:

$$M = \rho \int_{\Gamma_2} \varsigma dx, \qquad E = T_e + V$$
$$T_e = \frac{1}{2}\rho \int_{\Gamma} \Phi . \overline{\Phi} ds, \quad V = \frac{1}{2}\rho g \int_{\Gamma_2} \varsigma^2 dx \tag{32}$$

where M, T_e, V denote the mass of fluid, kinetic energy and potential energy respectively.

These figures show that the mass above the still water surface and the total energy become nearly constant after piston has stopped.

4. Conclusion

Based on a Lagrangian description and a finite difference method approximation of time derivatives, a boundary element algorithm is applied to analyze the problems of generation, deformation and breaking of solitary wave. Fig.3 through Fig.5 show that the numerical results are reasonable. It is found that breaking occurs about at $x/h = 16$, and the ratio of breaking height to breaking depth $\varsigma_b/h_b = 0.79$.

References

Chou, C. R., 1983. "The application of boundary element method to water wave mechanics," National Taiwan College of Marine Science and Technology, Harbor and Ocean Eng. Press (in Chinese).

Chou, C. R., Shih, R. S. and Fang, H.M., 1996. "Defoemation of

solitary wave in coastal zones," *Proc. Of the 7th Japan-China symposium on Boundary Element Method*, Elsevier Press, pp. 171~180.

Ckou, C. R. and Shih, R. S., 1996. "Generation and deformation of solitary waves," *China Ocean Engineering*, China Ocean Press, Vol. 10, No. 4, pp. 419-432.

Grilli, S. T., Subramanya, R., Svendsen, I. A., and Veeramony, J., 1994, "Shoaling of solitary waves on plane beaches," *J. of Waterway, Port, Coastal, and Ocean Engineering*, Vol. 120, No. 6, pp. 609~628.

Johson, R. S., 1972, "Some numerical solutions of a variable-coefficient Korteweg-de Vries equation (with applications to solitary wave development on a shelf)," *J. Fluid Mech.*, No. 54, pp. 81~91.

Madsen, O. S. and Mei, C. C., 1969, "The transformation of a solitary wave over an uneven bottom," *J. Fluid Mech.*, No. 39, pp. 781~791.

Nakayama, T., 1983, "Boundary element analysis of nonlinear water wave problem," *International journal for numerical method in engineering*, No. 19, pp. 953~970.

Sugino, R. and Tosaka, N., 1990, "Boundary element analysis of nonlinear water wave problem," *Pacific Congress on Marine Science and Technology*, pp. 18~25.